SIMULATIONS OF ALPHA PARAMETERS IN A TFTR DT SUPERSHOT WITH HIGH FUSION POWER

R.V. BUDNY, M.G. BELL, A.C. JANOS, D.L. JASSBY,
L.C. JOHNSON, D.K. MANSFIELD, D.C. McCUNE, M.H. REDI, J.F. SCHIVELL,
G. TAYLOR, T.B. TERPSTRA, M.C. ZARNSTORFF, S.J. ZWEBEN
Princeton Plasma Physics Laboratory,
Princeton University,
Princeton, New Jersey,
United States of America

ABSTRACT. A TFTR supershot with a plasma current of 2.5 MA, a neutral beam heating power of 33.7 MW and a peak DT fusion power of 7.5 MW is studied using the TRANSP plasma analysis code. Simulations of alpha parameters such as the alpha heating, pressure and distributions in energy and $v_\parallel/v$ are given. The effects of toroidal ripple and mixing of the fast alpha particles during the sawteeth observed after the neutral beam injection phase are modelled. The distributions of alpha particles on the outer midplane are peaked near forward and backward $v_\parallel/v$. Ripple losses deplete the distributions in the vicinity of $v_\parallel/v \approx -0.2$. Sawtooth mixing of fast alpha particles is computed to reduce their central density and broaden their width in energy.

1. INTRODUCTION

Experiments with deuterium–tritium (DT) plasmas were started in TFTR during 1993 [1–3]. Several experiments have been dedicated to maximizing the fusion power. In November 1994, DT discharges with neutral beam injection (NBI) heating of $P_{NBI} = 39$ MW, plasma currents of 2.7 MA and toroidal fields of 5.6 T achieved fusion power at peak rates up to 10.7 MW and at peak power densities above 2.5 MW/m^3.

The previous record was set in May 1994, when DT discharges with NBI heating of 34 MW, plasma currents of 2.5 MA and toroidal fields of 5.1 T achieved fusion power at peak rates up to 9.2 MW [4]. The discharge with the highest peak rate disrupted, but similar discharges with peak rates up to 7.5 MW did not disrupt and had sustained high fusion power production for approximately 0.5 s. Analysis of the highest non-disruptive discharge from May 1994 with a peak rate of 7.5 MW is discussed in this paper.

This discharge has been extensively modelled using the TRANSP time dependent plasma analysis code [5–8]. The modelling provides calculations of profiles of the deuterium and tritium densities, the hydrogenic isotopic mass, the fusion reactions, the fast ion parameters and the alpha heating. Results are in approximate agreement ($\sim 1\sigma$) with available measurements [5].

A detailed prediction for a DT supershot based on a moderate performance, reproducible, deuterium-only supershot was described before the DT campaign [7]. That simulation predicted 5.6 MW of fusion power with a fusion power ratio $Q_{DT} \equiv P_{DT}/P_{NBI} = 0.23$. This paper updates those simulations using an actual high performance DT discharge. One of the predictions [7] made before the DT campaign was that the stored energy in DT NBI supershots would be about 10% higher than in deuterium-only supershots. This predicted increase is due to changes in the NBI parameters, the effects of alpha electron heating and the additional stored energy of the alphas. The observed increase is twice as large [1]. The extra increase is attributed to an intrinsic isotopic scaling of the thermal plasma confinement with isotopic mass [8, 9].

Several methods are being used to measure facets of the confined alpha particle distributions in TFTR plasmas. One method uses charge exchange recombination spectroscopy of alphas excited by NBI ions [10]. Another method analyses the energy of neutral alpha particles from double charge exchange in pellet ablation clouds [11]. A third method is designed to analyse gyrotron Thomson scattering from alpha particles [12]. These diagnostics measure the alpha energy in different regions of energy and $\lambda \equiv v_\parallel/v \equiv \cos(\text{pitch angle})$. This paper gives simulations for the alpha distributions in energy and λ.

Supershots generally exhibit sawteeth before and after the NBI phase. These sawteeth are accompanied by significant decreases in the central plasma parameters such as T_e and n_e. If the fast ions are mixed during the sawtooth crashes, then the central neutron emission and

alpha parameters would be affected. Fast ion mixing is modelled in TRANSP and simulations of this mixing are being used to test empirically whether such mixing occurs.

General plasma conditions for the discharge are discussed in Section 2. The TRANSP modelling typically used for TFTR discharges is discussed in Section 3. Alpha particle parameters are discussed in Section 4. The fast alpha distributions are discussed in Section 5.

2. PLASMA CONDITIONS FOR SHOT 76 770

The neutral beams injected 19.6 MW of tritium and 14.1 MW of deuterium from 3.5 to 4.3 s. Plasma conditions at the time of peak neutron emission rate ($\approx$ 4.0 s) are I_p = 2.5 MA, B_{TF} = 5.1 T, R_0 = 2.5 m, a = 0.9 m and $q_\Psi(a)$ = 4. The q_Ψ profile was not measured, but $q_\Psi(0) \approx 0.8$ is typically measured in similar discharges. The total energy confinement time is 0.22 s. This relatively high confinement time resulted from intensive lithium pellet injection [13] into the ohmic phases of discharges during this experimental run in order to condition the vessel walls.

Supershots generally exhibit sawteeth during their ohmic phases, and occasionally during the neutral beam phase. Typical behaviour with high NBI power is that the pre-NBI sawteeth disappear after one or two crashes during the start of the NBI. After $\approx$ 0.1 s, sawteeth are generally not observed during the NBI except if the NBI power is low (< 25 MW) and the plasma current I_p is high (> 2 MA). They start about 0.2 s after the termination of NBI with regularity. Examples of the effects of sawteeth and the lithium pellet for shot 76 770 are seen in the $T_e(0)$ trace in Fig. 1. Empirical evidence for the degree to which the beam ions and fusion alpha ions are mixed during sawtooth crashes is not fully established. This mixing is computed to have significant consequences on the energy and pitch angle distributions of the fast ions.

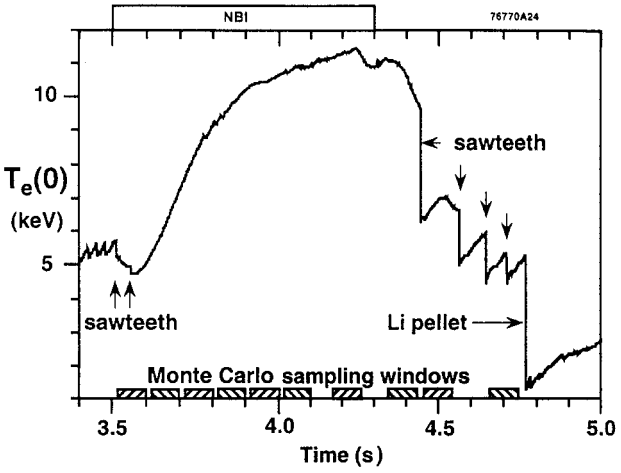

FIG. 1. Evolution of the central electron temperature measured from ECE. The sawtooth and pellet effects on $T_e(0)$ are indicated. The sampling windows employed for averaging the Monte Carlo data used for the fast ion distributions are also indicated.

There is little direct evidence for alpha particle effects on the plasma in supershots. One indirect piece of evidence is that the measured alpha losses are normal in supershots that do not have excessive MHD activity [14]. The measured rates of fast alpha particles collected in detectors at poloidal angles 20° [15] and 90° below the midplane for shot 76 770, normalized to the total neutron emission rate, are approximately constant in time.

3. TRANSP MODELLING CAPABILITIES

The TRANSP plasma analysis code is used to model the time evolutions of plasma parameters. The energy, particle, and magnetic field dynamics are computed. Measured plasma profiles and the location of the last closed flux surface are specified. Three temperatures (T_e, hydrogenic ion T_i and impurity ion T_x) are modelled. Typically, measurements of the electron temperature (from ECE) and of the temperature and the toroidal rotation velocity of the trace carbon impurity (from neutral-beam-induced charge exchange recombination spectroscopy) are used as initial inputs. The hydrogenic temperature T_i is computed from the measured T_x in TRANSP [6]. This computed central T_i is lower than T_x by several kiloelectronvolts. The difference is largest during the first ~ 0.2 s of the NBI.

Up to five thermal ion species and one impurity species can be modelled simultaneously in TRANSP. For the modelling described here, the thermal species are H, D, T, ^{4}He, Li and one heavier impurity. The hydrogen and impurity species are non-negligible components, as discussed in Ref. [5]. The lithium has small relative concentrations during the NBI phase. The helium ash is estimated to have small relative concentrations (peaking at $n_e/1000$ in the centre).

The equilibrium flux surfaces are calculated by solving the fixed boundary Grad–Shafranov equations using the total (beam + thermal) pressure. Typically ~ 6 s of the discharge evolution are modelled, starting within 0.5 s of the discharge initiation and continuing through the NBI. Modelling the early phase allows a more accurate computation of the magnetic field diffusion and the q_Ψ profile.

3.1. Fast ions

Monte Carlo techniques [16] are used to compute the deposition of the neutral beams, and the distributions of the beam ions and fusion ions. The beam ions and fusion products are assumed to slow down either classically or with an added anomalous radial diffusivity. The assumptions of classical slowing down and loss have been checked in the cases of beam ions [17] and DD fusion products [18]. For instance, if a constant radial diffusivity of $\sim 0.05\ m^2/s$ is assumed to be superimposed on the classical slowing down of the beam ions, then the TRANSP results for the total neutron rates and the stored energies would differ significantly from the measurements [17]. We extrapolate these results by assuming no anomalous diffusion for the fast alpha particles. The losses of beam ions and alpha particles on orbits that intercept the limiter or wall are computed using TRANSP.

The TRANSP modelling is tested and confirmed by comparing simulations with measurements. Examples of comparisons are the Shafranov shifts, the stored energy and the neutron emission profile. These tests are interrelated and provide global checks of the modelling. For instance, the Shafranov shifts, which depend on the total pressure, affect the plasma profiles that are used to calculate the plasma and beam pressures. Comparisons are discussed in detail in Ref. [5].

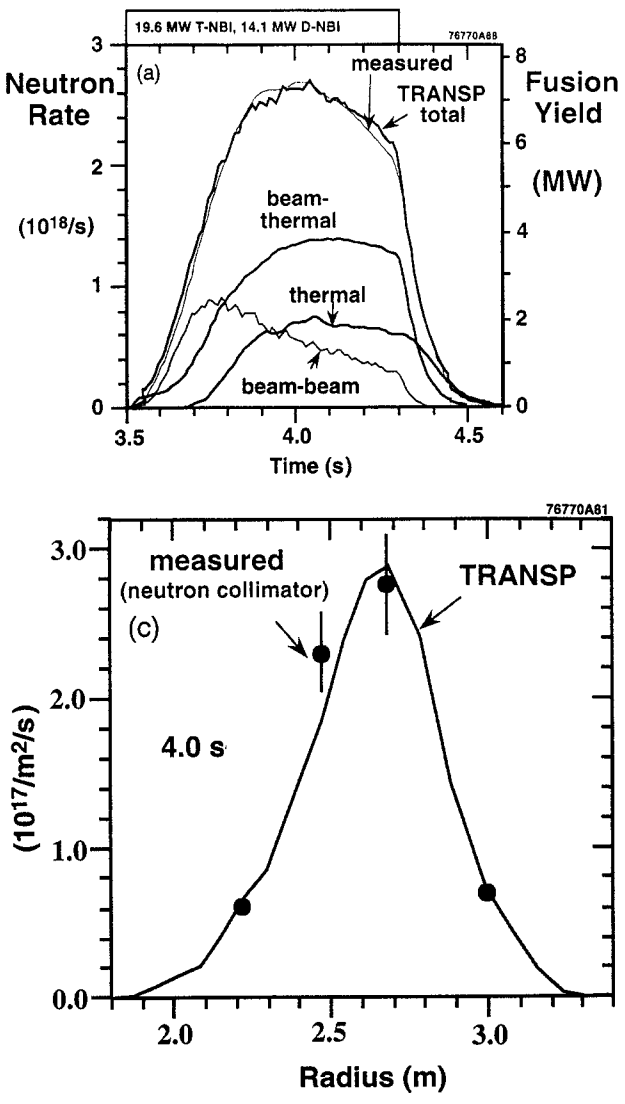

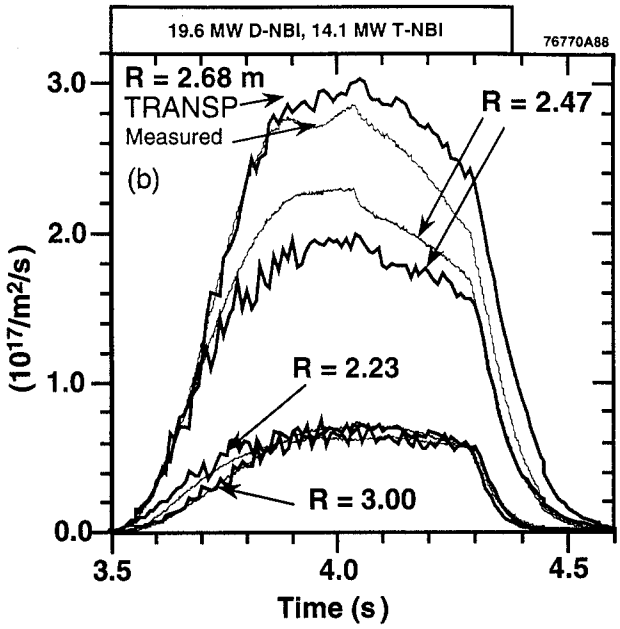

FIG. 2. Evolutions of: (a) the measured and simulated total neutron emissivities and the simulated contributions from beam–thermal, beam–beam and thermonuclear fusion reactions; (b) comparisons of the measured and simulated chordal neutron emissivities; (c) profiles near the time of peak neutron emission.

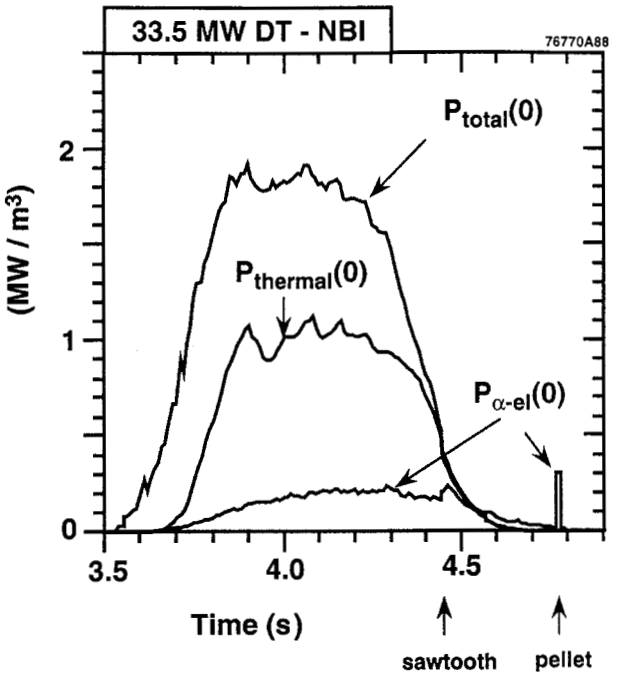

FIG. 3. Evolutions of the central fusion power densities of the total DT reactions, of the thermonuclear reactions and of the alpha electron heating. Fast ion mixing was not assumed for these results.

3.2. Neutron emission

The measured and simulated total neutron emission rates are shown in Fig. 2(a). (The absolute measurement uncertainty is given by $1\sigma \approx 7\%$.) These are in good agreement for the first 0.6 s of NBI. Later, the simulated total is systematically higher than the measured value. The neutron emission chordal profiles are measured by a collimator array. The absolute measurement error is given by $1\sigma \approx \pm 15\%$. Time evolutions of the simulations and measurements are compared in Fig. 2(b). Profiles near the time of peak emission are compared in Fig. 2(c). The simulated profiles are shifted several centimetres outward with respect to the measured profiles. Accurate simulations of the central neutron emission rates are desired since the alpha parameters depend sensitively on the central fusion rate. The simulation depends sensitively on the Z_{eff} value of the plasma, which is not known accurately for reasons discussed in Ref. [5].

3.3. Fusion power

The peak neutron emission rate is $S_n = 2.7 \times 10^{18}\ s^{-1}$, so the fusion yield, P_{DT} ($\equiv S_n/3.55 \times 10^{17}$ [MW/s]) is 7.5 MW. The calculated fraction of the total from thermonuclear reactions is 25%. The central fusion power density is dominantly thermonuclear, as shown in Fig. 3. The central alpha electron heating rate is shown for comparison. Its peak occurs after the peak fusion rate. This is discussed in more detail in Section 4.

3.4. Ripple effects

A model for estimating toroidal field ripple effects of fast ions has been included in TRANSP [19, 20]. The magnitude of the toroidal field ripple is used as an input along with a threshold set as a factor times the Goldston–White–Boozer [21] stochastic ripple threshold. When the turning points of fast ion orbits are at locations where the toroidal field ripple is above this threshold, the ions are ejected from the plasma. The choice of the multiplier has been adjusted by comparisons between TRANSP and guiding centre code calculated losses.

3.5. Sawteeth

The occurrence of sawteeth in TFTR supershots is consistent with a criterion of drift frequency, ω_* stabilization of the collisionless $m = 1$ reconnection mode [22, 23]. Sawteeth may have important implications for alpha parameters owing to mixing. TRANSP uses a phenomenological sawtooth model that is invoked at the observed sawtooth crash times if $q_\Psi(0)$ is less than 1. The magnetic flux surfaces are shifted using the Kadomtsev helical flux mixing model [24]. The calculated mixing radius is $\approx 30\%$ larger than the calculated $q_\Psi = 1$ radius.

The amount of current mixing can be adjusted in TRANSP to less than the full current mixing in the standard Kadomtsev model. A weighted average of the unmixed and fully mixed current profiles is imposed after the crash. For the results given here the weighting is 70% of the unmixed current and 30% of the fully mixed current. This amount of current mixing predicts $q_\Psi(0)$ values in approximate agreement with observations. Full (100%) current mixing predicts $q_\Psi(0)$ values that increase after the sawtooth crashes to values that are too high (close to 1) for consistency with measurements [25]. The sawtooth prescription in TRANSP generally calculates the $(m,n) = (1,1)$, (4,3) and (3,2) surfaces, which are within $\sim$ 5 cm of the locations of sawtooth inversions and of coherent MHD activity indicated by fast T_e measurements.

TRANSP can be run either with or without fast ion mixing. In the case where the fast ions are assumed to mix, the ions are shifted with the flux surfaces conserving helical flux. The poloidal angle for each Monte Carlo ion

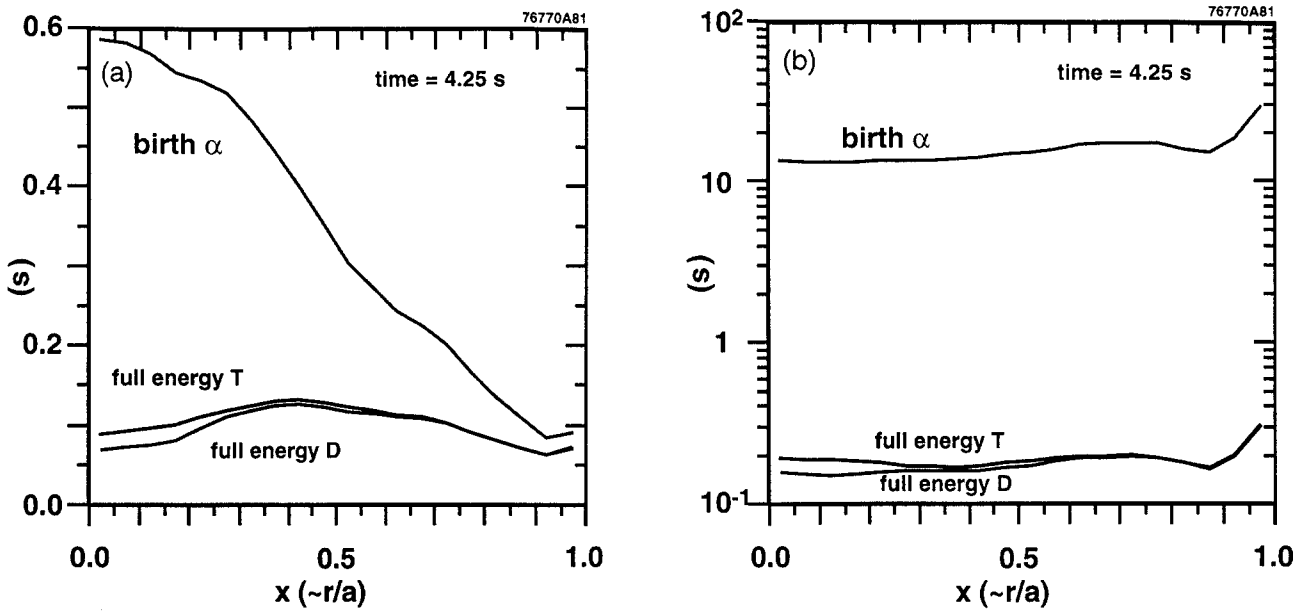

FIG. 4. Profiles of: (a) the slowing down times and (b) the pitch angle scattering times of the alpha particles and beam ions at birth.

is randomized and the values of $v_\parallel$ and $\mu \equiv v_\perp^2/B$ are conserved through the crash. This prescription alters the energies and the $\lambda \equiv v_\parallel/v$ value of the fast ions and converts some of the passing ions to trapped ions and vice versa.

4. ALPHA PARAMETERS

The alpha slowing down and pitch angle scattering are modelled. The slowing down and pitch angle scattering times are considerably longer than the corresponding times for beam ions, as shown in Figs 4(a, b). The confined alphas are calculated as mainly heating electrons. The alpha electron heating is predicted to be a significant portion of the total electron heating in the centre. Its profile is compared with the beam-electron and thermal-ion electron heating in Fig. 5.

The calculated time evolutions of the central fast alpha particle density n_α, average energy $\langle E_\alpha \rangle$, toroidal beta β_α and electron heating power are shown in Figs 6(a, b). During the NBI phase $n_\alpha(0)$ increases steadily, while $\langle E_\alpha(0) \rangle$ decreases. These contrary trends cause $\beta_\alpha(0)$ to peak during the NBI. Results are given with and without fast ion mixing. If the ions are assumed to mix during the sawtooth crash with the prescription described in Section 3, these central parameters decrease precipitously after the crash. If the ions are not mixed by sawteeth, these central parameters tend to decrease gradually after the termination of NBI. In this case, the alpha heating peaks during the sawtooth crashes and during the pellet (owing to the rapid thermalization in the high density pellet cloud).

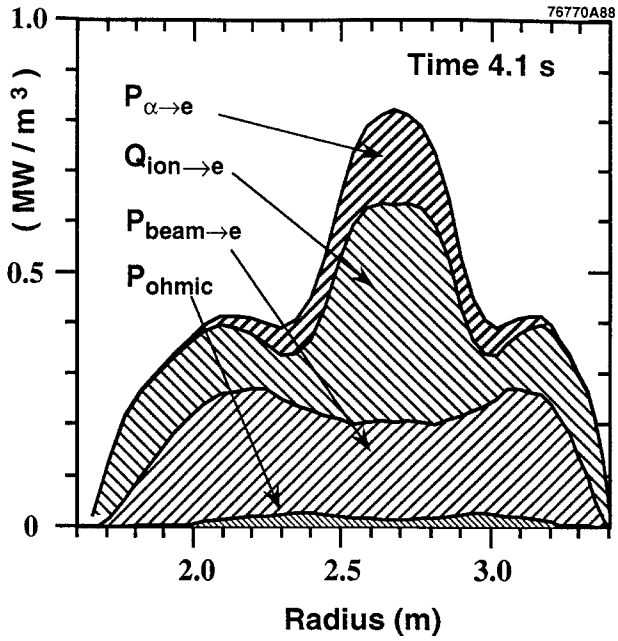

FIG. 5. Profiles versus major radius of the dominant electron heating terms showing significant central alpha electron heating.

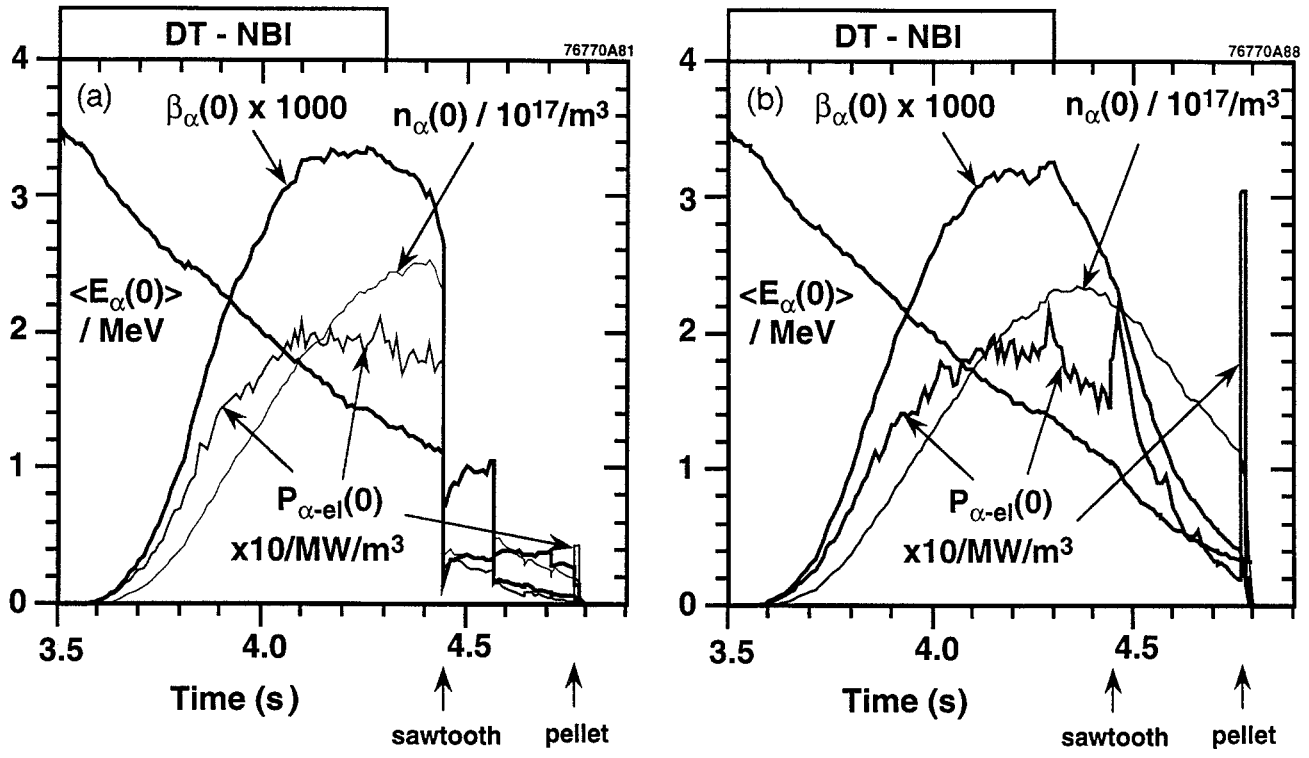

FIG. 6. Evolutions of central alpha parameters assuming: (a) fast ion sawtooth mixing and (b) no fast ion sawtooth mixing. The differences in the time evolutions before the post-NBI sawtooth are due primarily to Monte Carlo fluctuations.

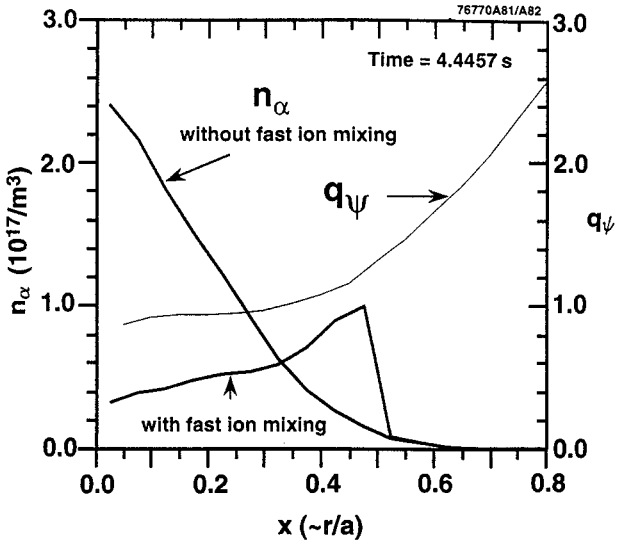

FIG. 7. Profiles of the fast alpha density and q_ψ after the first post-NBI sawtooth. The independent variable is the square root of the normalized toroidal flux (approximately r/a). The effect of sawtooth mixing on the alphas is shown. With the mixing prescription generally used for modelling TFTR discharges, the effect of sawtooth crashes on q_ψ is negligible.

The fast ion mixing prescription described above has dramatic effects on the fast ion profile, as shown in Fig. 7. The independent variable is the square root of the normalized toroidal flux, x. This variable is close in value to the normalized minor radius, r/a.

The ripple model predicts effects on alpha parameters that are more subtle than the sawtooth mixing. Profiles are shown in Figs 8(a, b). The ripple losses of energy for the alphas, deuterium-beam ions and tritium-beam ions are 9, 13 and 14%, respectively. The particle losses are 50–300% higher. The first orbit losses are relatively small ($\approx$ 3%), since the plasma current is relatively high (2.5 MA).

5. ALPHA DISTRIBUTIONS

Monte Carlo methods are used to track orbits of individual fast ions. The parameters for these can be sampled to generate their distribution in the laboratory rest frame,

$$\frac{\mathrm{d}f_j(E_j,\lambda_j,x,t)}{\mathrm{d}V\mathrm{d}E_j}$$

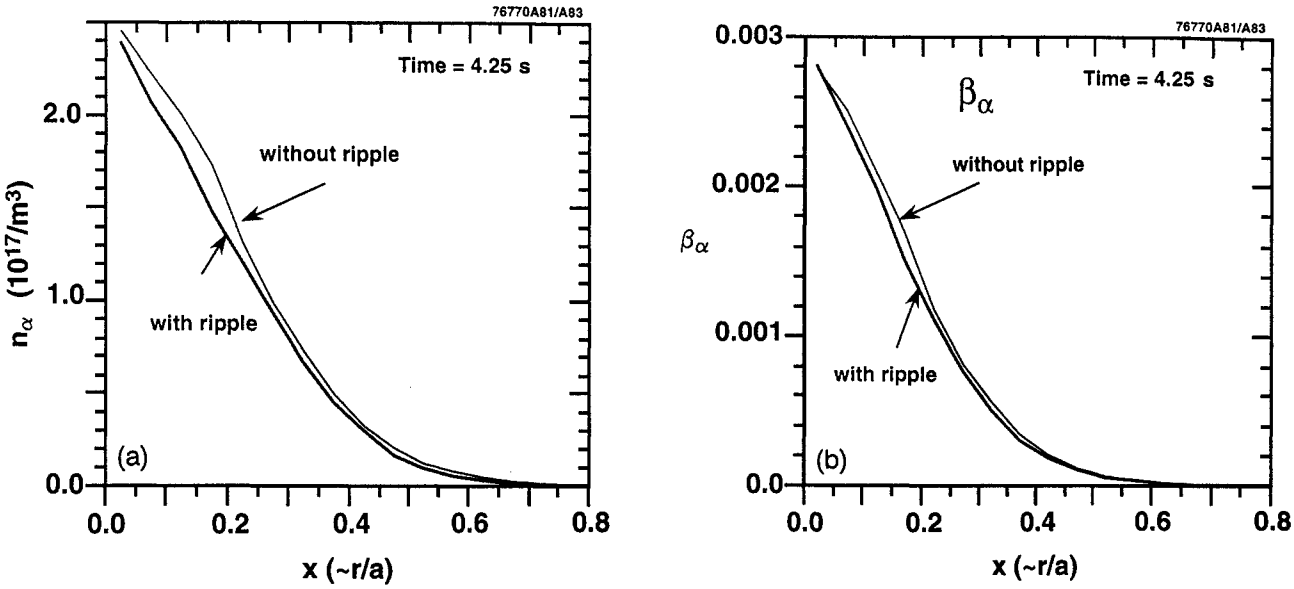

FIG. 8. Profiles of (a) the fast ion density and (b) β_α near the end of the NBI phase. The effects of ripple loss are indicated.

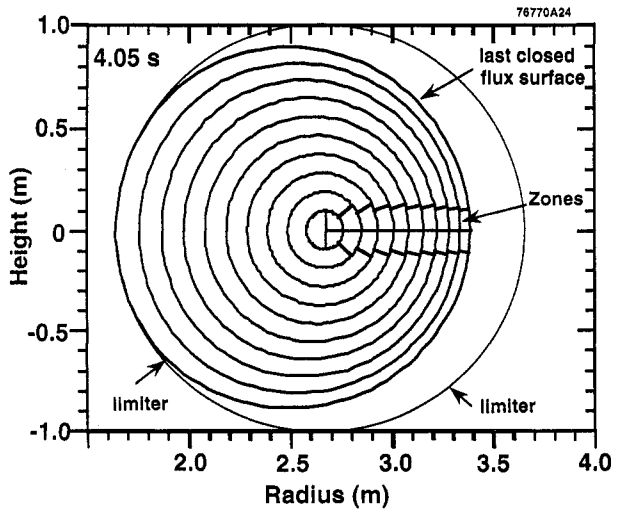

FIG. 9. Zones used for computing fast ion distributions. The radial intervals are determined by combining adjacent pairs of the 20 flux surfaces computed by TRANSP in solving for the MHD equilibrium. The poloidal angles are equally spaced within each flux surface and the number of poloidal angle increments increases as the flux increases. The zones for sampling the distributions on the outer midplane are indicated. Pairs of poloidal zones, one below and one above the midplane, are combined for the results presented here.

The independent variables are the energy E_j of the fast species j, $\lambda_j \equiv v_\parallel/v \equiv$ cos(pitch angle) with $v_\parallel$ the component of v in the direction of the field (with the sign given by the direction of the plasma current), and the location in space and time. In TFTR, the plasma current flows counterclockwise, viewed from above, and the toroidal field is clockwise. The distributions are normalized so that their integrals over E_j and averages over λ_j give the fast ion spatial density. An example of the flux-surface average of this spatial density is shown in Fig. 8(a).

These distributions are computed in TRANSP by counting the fast ions passing through the zones in a two dimensional slice at fixed toroidal angle. For the results given here, 100 equal energy intervals and 50 equal λ intervals are used. The zones are chosen to lie along the outer midplane. The radial spacing of the zones is in equal intervals of x. The poloidal widths of the zones are indicated in Fig. 9. The distributions are not the same as the orbit averages for the fast ions.

The results given here are from TRANSP runs using 8000 Monte Carlo deuterium and tritium beam ions, and 8000 fusion alpha ions. The results are averaged over 80 ms at various times during the discharge. These times are selected throughout the NBI phase, before and after the post-NBI sawteeth, and before the post-NBI pellet. The sampling windows are shown in Fig. 1.

The results for the beam ion distributions, f_D and f_T, and for f_α, are qualitatively similar to the results given in Ref. [7]. More detailed results for f_α are given here. First we show the effects of ripple by comparing f_α before the first post-NBI sawtooth. The plots in Figs 10(a, b) compare $f_\alpha(E_\alpha,\lambda,x = 0.5, t = 4.43$ s) calculated with and without the ripple model. The results for both

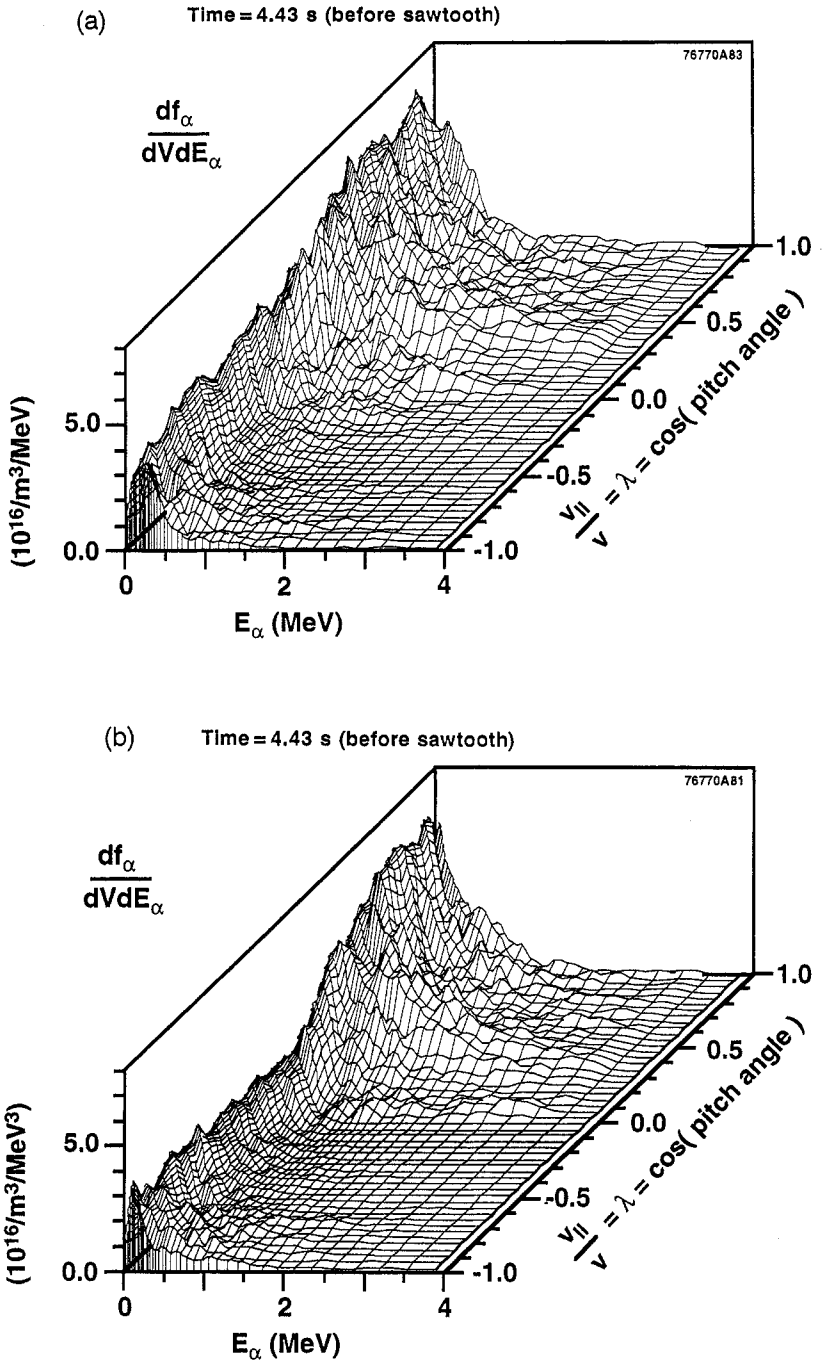

FIG. 10. Distribution of fast alphas in E *and* λ *at the half-radius, just before the first post-NBI sawtooth crash. For (a) the ripple model is assumed to be negligible. For (b) the usual ripple model is used. The distributions are averaged over energy using a width of 0.1 MeV.*

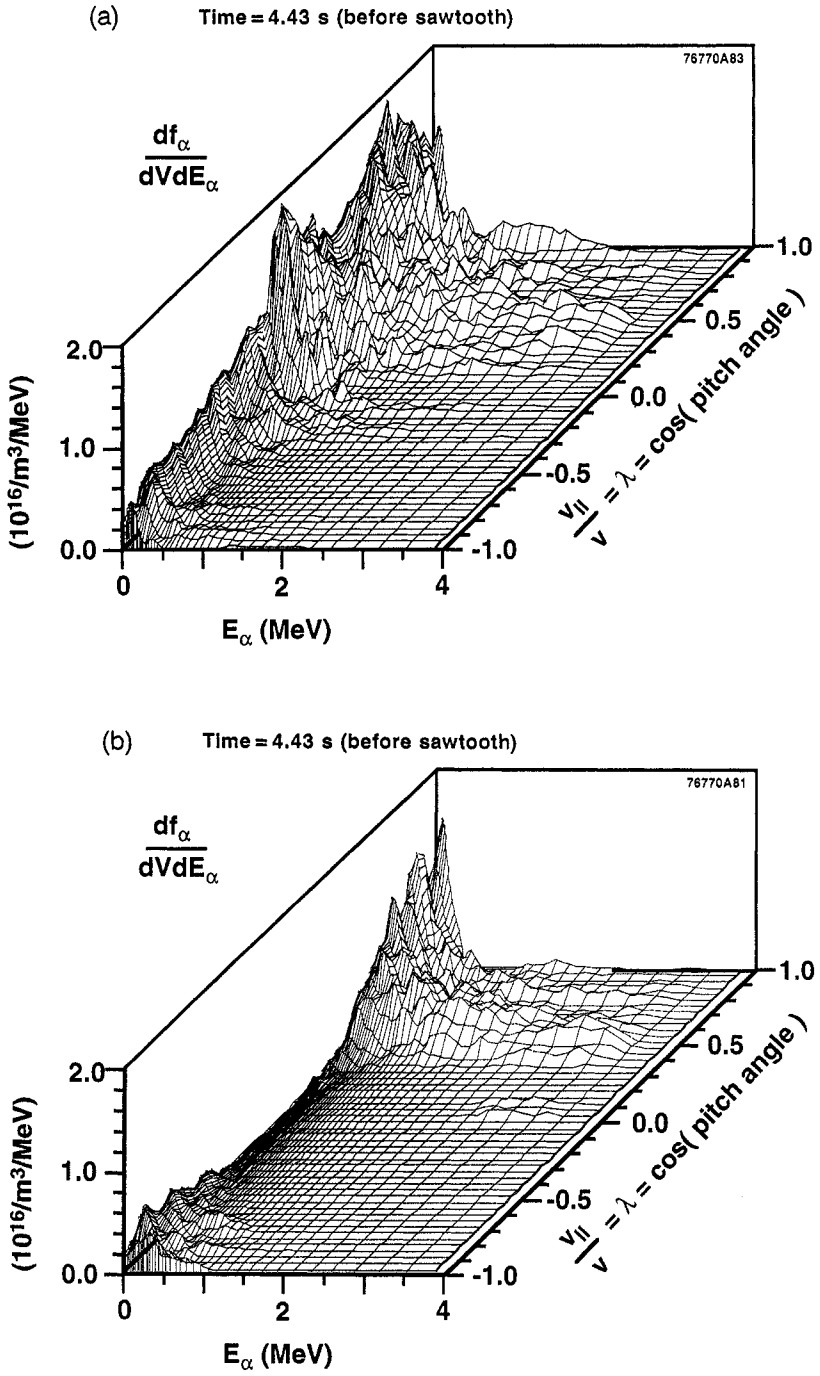

FIG. 11. Distribution of fast alphas in E *and* λ *at* x = *0.7, just before the first post-NBI sawtooth crash. For (a) the ripple model is assumed to be negligible. For (b) the usual ripple model is used. The distributions are averaged over energy using a width of 0.1 MeV.*

cases show a peaking at positive λ. This is due to non-zero orbit effects and the λ peaking of the beam ion distributions. The alpha distributions have regions with relatively low values near $\lambda \approx -0.4$ and $E_\alpha \approx 2.5$ MeV.

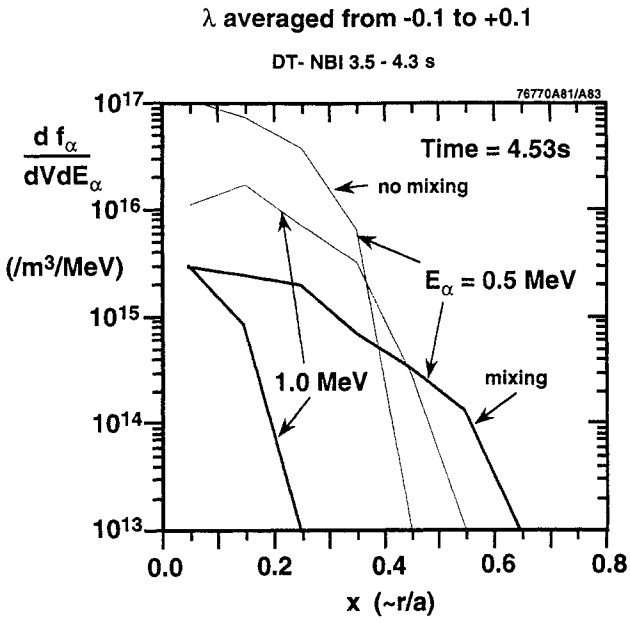

FIG. 12. Distribution of fast alphas over x with λ near 0.0 and E_α = 0.5 and 1.0 MW, just after the first post-NBI sawtooth crash. Two cases are compared: (a) the fast ion sawtooth mixing and the ripple losses are assumed to be negligible, and (b) the usual fast ion mixing and ripple models are used.

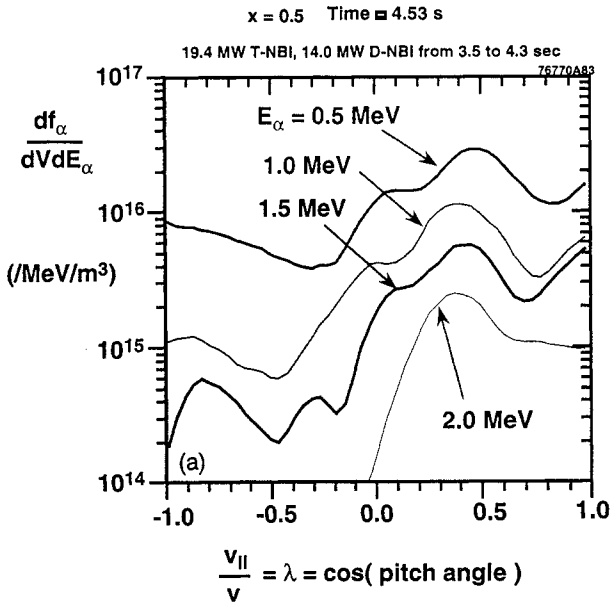

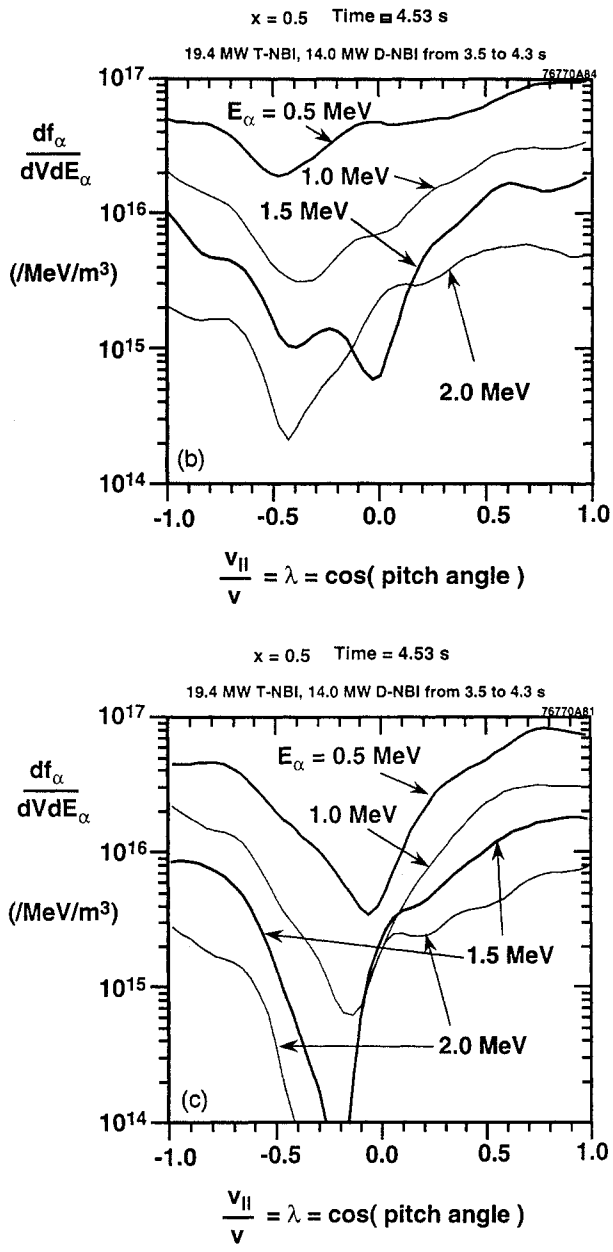

FIG. 13. Distribution of fast alphas in λ at x = 0.5, just after the first post-NBI sawtooth crash. The results are averaged over λ, with Δλ = 0.2. Three cases are compared: (a) the fast ion sawtooth mixing and the ripple losses are assumed to be negligible, (b) the usual fast ion mixing model is used, (c) the usual fast ion mixing and ripple models are used.

This is a consequence of the trapped ions with negative λ on the midplane having banana orbits with x increasing away from the midplane, whereas those with positive λ have banana orbits with x decreasing away from the midplane. Some of the orbits with increasing x leave the last closed flux surface and can get scraped off by the limiter.

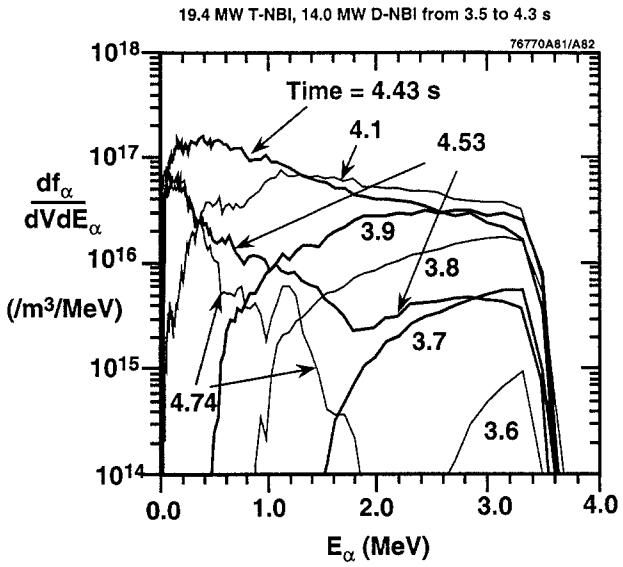

FIG. 14. Broadening of the alpha distribution, averaged over λ in the centre, assuming fast ion sawtooth mixing and the usual ripple losses.

In addition, the slowing down time decreases with x, as shown in Fig. 4(a), so the ions with negative λ slow down more rapidly. In the case where the ripple model is turned on (Fig. 10(b)), this depletion is more pronounced since the ripple loss is more likely at large R where the ripple threshold is lower. These effects are seen to a lesser extent in the centre ($x \approx 0$), and to a larger extent at $x > 0.5$. At $x \approx 0.7$ these effects are very pronounced, as shown in Figs 11(a, b).

The effects of fast ion sawtooth mixing can bee seen in the distributions after the sawtooth crashes. Effects on the energy distribution are shown in Figs 12(a, b). The results are averaged from 4.52 to 4.53 s and for $-0.1 < \lambda < 0.1$. The mixing has the effect of depleting the distribution at $x = 0$ and increasing it at $x = 0.5$. The mixing and ripple effects on the pitch angle distribution at $x = 0.5$ are shown in Figs 13(a–c). Their combined effects cause a trough near $\lambda \approx -0.2$.

Thermal Doppler broadening in E_α of f_α is not yet included in TRANSP; however, the broadening due to the alphas slowing down and scattering is included. The broadening in the centre ($x = 0$) is shown in Fig. 14. During the first 0.5 s of NBI the distribution is inverted. Later it develops into a slowing down distribution. Both ripple and sawtooth mixing effects are included in this result.

6. SUMMARY

Simulations of alpha parameters using TRANSP are given for a high performance, non-disruptive TFTR DT NBI supershot with a peak fusion power of 7.5 MW. Effects of ripple loss and sawteeth are modelled. Trapped fast ions are assumed to be ejected from the plasma if their turning points are above a preset factor times the Goldston–White–Boozer threshold. The ripple losses of alpha particles are estimated to be ≈ 10% for the plasma discussed in this paper. The sawtooth model in TRANSP for the thermal plasma is a modification of the Kadomtsev flux and current mixing model. In TFTR discharges, the amount of current mixing that gives q_Ψ profiles in approximate agreement with measurements is about 30%. A model for fast ion mixing during the sawtooth crashes is also incorporated in TRANSP. Their guiding centres are assumed to remain on the flux surfaces, and their parallel velocity is assumed to be conserved. Results with and without fast ion mixing during the post-NBI sawteeth are compared. The central alpha density and pressure are predicted to decrease significantly if the fast ions mix during sawteeth.

Monte Carlo methods are used to calculate fast ion distributions. Results are given for the distributions on the outer midplane versus energy and λ = cos(pitch angle). The central beam ion distributions in λ are peaked near forward and backward pitch angles. Ripple losses deplete regions with $\lambda \approx -0.2$ and $E \approx 2.5$ MeV. Sawtooth mixing of the fast alpha particles is predicted to alter the pitch angle distributions.

ACKNOWLEDGEMENTS

We wish to thank J.D. Strachan for encouragement and the USDOE for support under Contract No. DE-AC02-76-CHO-3073.

REFERENCES

[1] HAWRYLUK, R.J., et al., Phys. Rev. Lett. **72** (1994) 3530.
[2] STRACHAN, J.D., et al., Phys. Rev. Lett. **72** (1994) 3526.
[3] STRACHAN, J.D., et al., Plasma Phys. Control. Fusion **12** (1994) 33.
[4] BELL, M.G., et al., in Plasma Physics and Controlled Nuclear Fusion Research 1994 (Proc. 15th Int. Conf. Seville, 1994), Vol. 1, IAEA, Vienna (1995) 171.
[5] BUDNY, R.V., et al., Analysis of High Fusion Power TFTR Supershots, Rep. PPPL-3039, Princeton Plasma Phys. Lab., NJ (1994).
[6] BUDNY, R.V., et al., Nucl. Fusion **32** (1992) 429.
[7] BUDNY, R.V., Nucl. Fusion **34** (1994) 1247.
[8] BUDNY, R.V., et al., in Controlled Fusion and Plasma Physics (Proc. 21st Eur. Conf. Montpellier, 1994), Vol. 18B, Part I, European Physical Society, Geneva (1994) 82.
[9] SCOTT, S.D., et al., Phys. Plasmas **2** (1995) 2299.
[10] McKEE, G., et al., Phys. Rev. Lett. **75** (1995) 649.

[11] FISHER, R., et al., Phys. Rev. Lett. **75** (1995) 846; PETROV, M., et al., Nucl. Fusion **35** (1995) this issue.
[12] MACHUZAK, J., et al., Rev. Sci. Instrum. **66** (1995) 484.
[13] SNIPES, J.A., et al., J. Nucl. Mater. **196–198** (1992) 686.
[14] ZWEBEN, S.J., et al., Nucl. Fusion **35** (1995) 893.
[15] ZWEBEN, S.J., et al., Nucl. Fusion **35** (1995) this issue.
[16] GOLDSTON, R.J., et al., J. Comput. Phys. **43** (1981) 61.
[17] RUSKOV, E., et al., Nucl. Fusion **35** (1995) 1099.
[18] STRACHAN, J.D., et al., Tritium Burnup Profile Measurements (in preparation).
[19] REDI, M.H., et al., Nucl. Fusion **35** (1995) 1191.
[20] REDI, M.H., et al., Nucl. Fusion **35** (1995) this issue.
[21] GOLDSTON, R.J., et al., Phys. Rev. Lett. **47** (1981) 647.
[22] LEVINTON, F.M., et al., Phys. Rev. Lett. **72** (1994) 2895.
[23] ZAKHAROV, L., et al., in Plasma Physics and Controlled Nuclear Fusion Research 1994 (Proc. 15th Int. Conf. Seville, 1994), Vol. 3, IAEA, Vienna (in press) Paper D-19.
[24] KADOMTSEV, B.B., Sov. J. Plasma Phys. **1** (1975) 389.
[25] YAMADA, M., et al., Phys. Plasmas **1** (1994) 3269.

(Manuscript received 6 June 1995
Final manuscript accepted 18 October 1995)